

Collision-Induced Dissociation of Mobility-Separated Ions Using an Orifice-Skimmer Cone at the Back of a Drift Tube

Young Jin Lee, Cherokee S. Hoaglund-Hyzer, John A. Taraszka, Gina A. Zientara, Anne E. Counterman, and David E. Clemmer*

Department of Chemistry, Indiana University, Bloomington, Indiana 47405

An ion mobility-mass spectrometry technique that incorporates a differentially pumped orifice-skimmer cone (OSC) region at the exit of the drift tube has been developed. The OSC region is similar in design to those used in electrospray ionization sources and offers improvements in ion transmission (by factors of ~5–10 compared with previous designs) and the ability to induce fragmentation of mobility-separated ions. The separation of ions prior to dissociation at the skimmer cone allows the origin of fragment ions to be examined. Here, we describe the experimental design and demonstrate the approach by examining fragment ions that are common to multiple charge states and different gas-phase ion conformations of electrosprayed angiotensin II and [Sar¹, Val⁵, Ala⁸] angiotensin II peptides.

A common design feature of many electrospray ionization (ESI)¹ sources is a differentially pumped orifice-skimmer cone (OSC) region between the atmospheric pressure spray and the low-pressure mass spectrometry (MS) chamber. The intermediate pressure region (usually ~1–5 Torr) reduces pumping requirements in the low-pressure chamber, and acceleration of ions through this region provides a simple strategy for producing fragment ions. Currently, this approach is incorporated in the combination of ESI with many types of mass analyzers^{2,3} and is exploited in a number of commercial instruments.⁴

A limitation of fragment ion production in the source is that the process is ill defined; that is, the assignments of observed fragment ions with corresponding parent ions are often ambiguous. In this report, we describe the use of OSC dissociation at the back of a drift tube. Ion mobility techniques^{5,6} can distinguish between many types of ions that have identical mass-to-charge (m/z) ratios. The complementary use of ion mobility measure-

ments of parent ions with information about fragmentation processes that occur in the OSC region provides detailed insight into how different fragments are formed. Here, we illustrate the method by examining fragments that are common to multiple charge states of angiotensin II (NRVYIHPF) as well as different ion conformations of the $[M + 2H]^{2+}$ and $[M + 3H]^{3+}$ of [Sar¹, Val⁵, Ala⁸] angiotensin II.

The present experiments are related to other efforts to incorporate high-pressure ion separation methods with MS analysis. Our laboratory has developed an approach that utilizes an octopole collision cell between a drift tube and a time-of-flight MS instrument.^{7,8} In this approach, the coincidence of fragment drift times with their antecedent parents allows MS/MS analysis of mixtures of ions to be carried out in a parallel fashion. Additionally, the recent combination of the mobility/time-of-flight approach with a high-pressure matrix-assisted laser desorption/ionization source⁹ as well as the development of methods that take advantage of differences in the high- and low-field mobilities of ions¹⁰ are currently receiving considerable attention.

EXPERIMENTAL SECTION

General Information. A schematic diagram of the experimental apparatus is shown in Figure 1. The instrument is composed of three basic components: (1) an ESI source; (2) an injected-ion drift tube with a differentially pumped OSC region; (3) a quadrupole mass analyzer with an off-axis collision dynode/microchannel plate detector. Each component is described in more detail below. A brief overview of the experimental approach is as follows. Electrosprayed ions are extracted into a high-vacuum

- (1) Fenn, J. B.; Mann, M.; Meng, C. K.; Wong, S. F.; Whitehouse, C. M. *Science* **1989**, *246*, 64.
- (2) Smith, R. D.; Loo, J. A.; Barinaga, C. J.; Edmonds, C. G.; Udseth, H. R. *J. Am. Soc. Mass Spectrom.* **1990**, *1*, 53. Barinaga, C. J.; Edmonds, C. G.; Udseth, H. R.; Smith, R. D. *Rapid Commun. Mass Spectrom.* **1989**, *3*, 160. Meng, C. K.; McEwen, C. N.; Larsen, B. S. *Rapid Commun. Mass Spectrom.* **1990**, *4*, 151.
- (3) Katta, V.; Chowdhury, S. K.; Chait, B. T. *Anal. Chem.* **1991**, *63*, 174.
- (4) Lowery, K. S.; Griffy, R. H.; Kruppa, G. H.; Speir, J. P.; Hofstadler, S. A. *Rapid Commun. Mass Spectrom.* **1998**, *12*, 1957. van Dongen, W. D.; van Wijk, J. I. T.; Green, B. N.; Heerma, W.; Haverkamp, J. *Rapid Commun. Mass Spectrom.* **1999**, *13*, 1712.

- (5) Ion mobility spectrometry methods are discussed in the following references: Hagen, D. F. *Anal. Chem.* **1979**, *51*, 870. Tou, J. C.; Boggs, G. U. *Anal. Chem.* **1976**, *48*, 1351. Karpas, Z.; Cohen, M. J.; Stimac, R. M.; Wernlund, R. F. *Int. J. Mass Spectrom. Ion Processes* **1986**, *83*, 163. St. Louis, R. H.; Hill, H. H. *Crit. Rev. Anal. Chem.* **1990**, *21*, 321. von Helden, G.; Hsu, M. T.; Kemper, P. R.; Bowers, M. T. *J. Chem. Phys.* **1991**, *95*, 3835. Jarrold, M. F. *J. Phys. Chem.* **1995**, *99*, 11.
- (6) For recent reviews of ion mobility studies of biomolecules, see: Clemmer, D. E.; Jarrold, M. F. *J. Mass Spectrom.* **1997**, *32*, 577. Liu, Y.; Valentine, S. J.; Counterman, A. E.; Hoaglund, C. S.; Clemmer, D. E. *Anal. Chem.* **1997**, *69*, 728A.
- (7) Hoaglund-Hyzer, C. S.; Li, J.; Clemmer, D. E. *Anal. Chem.* **2000**, *72*, 2737.
- (8) Hoaglund-Hyzer, C. S.; Clemmer, D. E. *Anal. Chem.* **2001**, *73*, 177.
- (9) Gillig, K. J.; Ruotolo, B.; Stone, E. G.; Russell, D. H.; Fuhrer, K.; Gonin, M.; Schultz, A. J. *Anal. Chem.* **2000**, *72*, 3965.
- (10) Buryakov, I. A.; Krylov, E. V.; Nazarov, E. G.; Rasulev, U. K. *Int. J. Mass Spectrom. Ion Processes* **1993**, *143*. Purves, R. W.; Guevremont, R. *Anal. Chem.* **1999**, *2346*, 6.

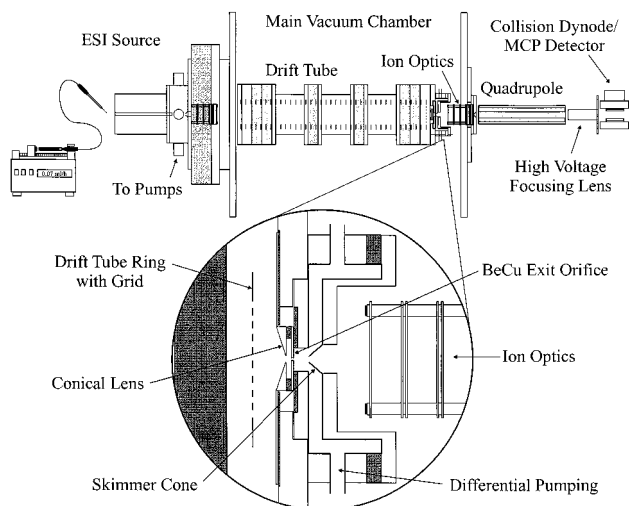


Figure 1. Schematic diagram of the injected-ion mobility-mass spectrometer. The inset shows the details associated with the differentially pumped orifice-skimmer cone region. See text for details.

region ($\sim 5 \times 10^{-5}$ Torr) and focused into an ion beam. Pulses of ions (50–150 μs in duration) are injected into a drift tube containing Ar buffer gas. Ions drift through the gas under the influence of a weak uniform electric field and are separated due to differences in their mobilities through the gas. Ions are extracted from the drift tube using a high-pressure focusing element (described below) directly into the differentially pumped OSC region. Ions are accelerated across this region and are subjected to energizing collisions that can induce fragmentation. Ions exit the OSC region into the low-pressure vacuum chamber, are focused into a quadrupole mass spectrometer, and are detected.

Ion Formation. Angiotensin II (human, 98% purity, from Novabiochem, San Diego, CA) and [Sar¹, Val⁵, Ala⁸] angiotensin II (97% purity, from Sigma, St. Louis, MO) were used for these studies. Positively charged (protonated) ions were formed by electrospraying solutions containing 10^{-4} – 10^{-5} M peptide solution in 49:49:2 (% v) water/acetonitrile/acetic acid. The ESI needle was biased +3800 V relative to the entrance of the desolvation region. Typical solution flow rates were 0.07 mL/h. Solutions were electrosprayed at atmospheric pressures into a stainless steel capillary (18.7 cm long) and then traveled through a differentially pumped desolvation region. This region is 5 cm long and is operated at a pressure of 1–2 Torr. Some of the ions exit the differentially pumped cavity through a 0.10-cm-diameter skimmer cone orifice and enter the main chamber of the instrument.

Injected-Ion Drift Tube and Differentially Pumped OSC Region. The present studies are carried out using an injected-ion drift tube that allows ions to be injected from high vacuum into the entrance of the high-pressure drift tube. The drift tube is 50.48 cm long with a 0.10-cm-diameter entrance aperture and a 0.20-cm exit aperture. The drift tube body is made of three stainless steel sections, an entrance plate, and an exit plate that are electrically isolated with ceramic spacers machined from Mycalex (McMaster Carr, Chicago, IL). Forty equally spaced 0.025-cm-thick BeCu rings are connected by a series of 5.00-M Ω high-vacuum resistors ($\pm 1\%$, from KDI Electronics, Whippany, NJ) in order to create a uniform electric field along the drift axis. A voltage drop along the outer sections of the drift tube is created

using 5.00-M Ω resistors. This reduces the voltage difference between the BeCu rings that create the drift field and the outer sections of the drift tube. Data were recorded using ~ 1 –2 Torr of 300 K Ar buffer gas and applied drift fields of 10–13 V $\cdot\text{cm}^{-1}$.

As ions are injected into the drift tube they are rapidly heated by initial collisions with the buffer gas. Further collisions cool the ions to the temperature of the buffer gas. The injection voltage is defined by the voltage difference between the exit plate of the high-pressure ESI source and the drift tube entrance plate. By varying the injection voltage, it is possible to induce conformational changes¹¹ as well as dissociation.¹² These changes can be monitored by measuring ion mobilities or mass spectra and provide information about folding and unfolding dynamics or fragmentation (sequence) information, respectively. The present studies were carried out using injection voltages from 70 to 150 V. The measured drift time is a composite of the time the ions spend in the drift tube and the time required for the ion pulse to travel through other portions of the instrument before reaching the detector. Because the residence time in other portions of the instrument is much shorter than the time spent in the drift tube, we refer to the time required to hit the detector as the drift time.

The inset in Figure 1 shows the details of the high-pressure focusing element and the differentially pumped OSC region.¹³ The high-pressure focusing element consists of a stainless steel conical lens and a 0.20-cm-diameter BeCu exit orifice lens. These electrodes are separated by a Teflon isolator and mounted on the inside of the drift tube exit plate. A Ni mesh (90% transmittance, from Buckbee-Mears, St. Paul, MN) grid is used in place of the last drift tube ring electrode in order to ensure a uniform drift field across all but the last 1.0 cm of the drift tube. As ions enter the region between the grid and the exit region they are focused by a nonuniform field (described below). The exit of the drift tube includes a differentially pumped region that extends from the exit plate of the drift tube to a 0.10-cm-diameter skimmer cone that is 6.5 mm from the drift tube exit orifice. The pressure in this region is monitored by a capacitance manometer (model 640A Baratron from MKS, Andover, MA) and is typically on the order of 0.05 Torr (under the experimental conditions employed). The OSC potential used for fragmentation studies is defined as the voltage difference between the BeCu orifice plate and the skimmer cone. In most cases, no fragmentation of precursor ions is observed when OSC potentials below ~ 10 V are used.

Figure 2 shows equipotential lines that are calculated by using typical experimental voltages on the electrodes in this region.¹⁴ A series of equipotentials having a balloonlike shape provides a means of focusing the diffuse ion cloud at the exit of the drift tube. Ion intensities are typically factors of 5–10 times greater

- (11) Clemmer, D. E.; Hudgins, R. R.; Jarrold, M. F. *J. Am. Chem. Soc.* **1995**, *117*, 10141. Shelimov, K. B.; Clemmer, D. E.; Hudgins, R. R.; Jarrold, M. F. *J. Am. Chem. Soc.* **1997**, *119*, 2240. Shelimov, K. B.; Jarrold, M. F. *J. Am. Chem. Soc.* **1997**, *119*, 2987. Woenckhaus, J.; Mao, Y.; Jarrold, M. F. *J. Phys. Chem. B* **1997**, *101*, 847. Woenckhaus, J.; Hudgins, R. R.; Jarrold, M. F. *J. Am. Chem. Soc.* **1997**, *119*, 9586. Valentine, S. J.; Clemmer, D. E. *J. Am. Chem. Soc.* **1997**, *119*, 3558. Valentine, S. J.; Anderson, J. G.; Ellington, A. D.; Clemmer, D. E. *J. Phys. Chem. B* **1997**, *101*, 3891. Valentine, S. J.; Counterman, A. E.; Clemmer, D. E. *J. Am. Soc. Mass Spectrom.* **1997**, *8*, 954.
- (12) Liu, Y.; Clemmer, D. E. *Anal. Chem.* **1997**, *69*, 2504.
- (13) This focusing element is similar in design to one used by Bowers, Weis, and co-workers (Kemper, P., personal communication).
- (14) Dahl, D. A. *SIMION (Version 6.0)*; Idaho National Engineering Laboratory: Idaho Falls, ID.

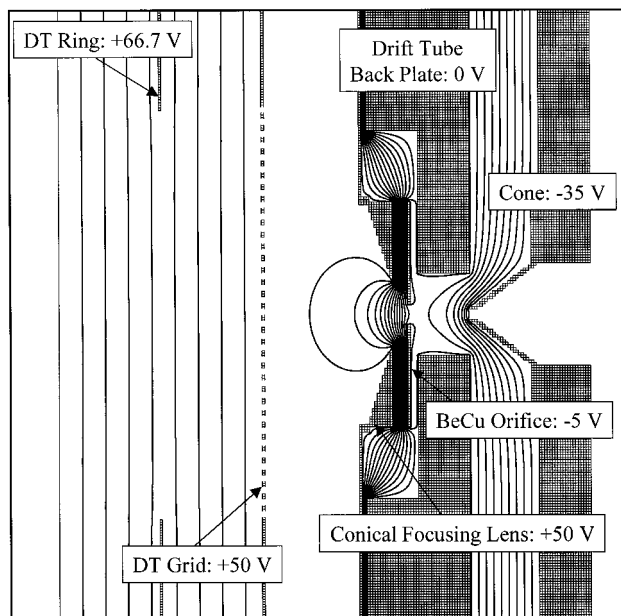


Figure 2. Equipotential lines in the back of the drift tube and the differentially pumped orifice-skimmer cone region as determined using SIMION (see ref 14). Only the final two drift tube rings of a total of 40 are shown. The last drift tube ring is a grid that is used to prevent field penetration from the conical lens assembly into the drift region. The voltages applied to each electrode used for the calculated field lines are indicated.

than intensities that are measured using a flat plate at the exit of the drift tube. The enhanced signal can be rationalized by considering the increased orifice size at the exit of the drift tube (made possible by the differential pumping region) and a focusing effect of the high-pressure conical lens assembly.

Mass Spectrometer and Detector. When ions exit the drift tube they are focused into a quadrupole mass filter (4000 amu range, from ABB Extrel, Pittsburgh, PA) that can be scanned to obtain a mass spectrum or fixed to transmit a specific m/z ion. Information about the origin of fragment ions formed in the OSC region is obtained by setting the quadrupole to transmit only the fragment of interest. In this case, the mobility distribution is an indication of all parent ions that lead to formation of the selected fragment. We refer to this type of data set as a *precursor ion mobility* (PIM) spectrum for the specified fragment.

Upon exiting the quadrupole, ions are detected by an off-axis collision dynode/microchannel plate assembly that was built in-house. The quadrupole and detector are housed in a separate differentially pumped chamber and typical pressures during these experiments are $\sim 1 \times 10^{-6}$ Torr.

RESULTS AND DISCUSSION

Influence of OSC Potential on the Mass Spectra of Electrosprayed Angiotensin II. Figure 3 shows typical mass spectra for angiotensin II under conditions where ions are accelerated through the OSC region using 5- or 30-V potential drops. Under the low-energy collision conditions in the OSC region, the mass spectrum is dominated by peaks centered at $m/z = 349.5$, 523.8, and 1046.5, consistent with formation of the $[M + 3H]^{3+}$, $[M + 2H]^{2+}$, and $[M + H]^+$ ions, respectively. As the OSC potential is increased, the relative abundances of the $[M + 3H]^{3+}$

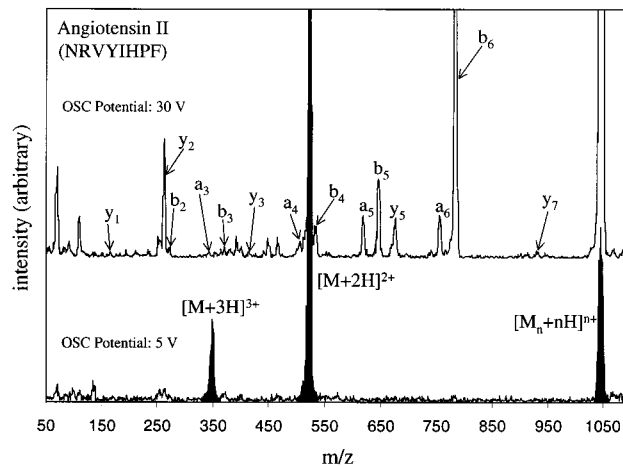


Figure 3. Mass spectra for angiotensin II (NRVYIHPF) at two different OSC potentials. The bottom spectrum is obtained using an OSC potential of 5 V. Under these conditions, the $[M_n + nH]^{n+}$, $[M + 2H]^{2+}$, and $[M + 3H]^{3+}$ ions dominate and little fragmentation is observed. The top spectrum is obtained using an OSC potential of 30 V. Peaks corresponding to fragment ions produced in the OSC region are observed. Assignments of peaks use the nomenclature given in ref 15 and are discussed in the text.

and $[M + 2H]^{2+}$ peaks decrease and an array of fragment peaks is observed. Most fragment peaks can be assigned as a-, b-, and y-type ions¹⁵ by comparison of measured m/z values with values expected for fragmentation of angiotensin II.¹⁶ Chait and co-workers³ previously used OSC fragmentation in an ESI source to examine angiotensin II; the present data obtained upon accelerating ions in the OSC region with a 30-V potential appear similar to the previous results.

Ion Mobility Distributions of Angiotensin II at Low OSC Potentials. More insight into the nature of the ions observed in the mass spectra shown in Figure 3 is obtained by examining the ion mobility distributions in Figures 4 and 5. Figure 4 shows ion mobility data recorded using a 5-V OSC extraction potential. Under these conditions, the ion mobility distribution for the $[M + 3H]^{3+}$ ion shows a single narrow peak at 4.82 ms. The distributions for the $m/z = 523.8$ and 1046.5 ions show substantially more complicated behavior. Data obtained for the $m/z = 1046.5$ ion shows a broad feature that extends from ~ 5.7 to 9.0 ms and a smaller feature, centered at ~ 10.24 ms. Data obtained in helium buffer gas (not shown) appear similar (although peaks are shifted). To assign these peaks, we have compared calculated mobilities for compact geometries generated by molecular modeling with the experimental results obtained in He as we have described in detail previously.^{17,18} This comparison shows that the peak at the longest drift time corresponds to a compact $[M + H]^+$ monomer ion. This assignment is consistent with observations we have

(15) The nomenclature for fragment formation is described by: Johnson, R. S.; Martin, S. A.; Biemann, K. *Int. J. Mass Spectrom. Ion Processes* **1988**, *86*, 137.

(16) Assignments were made by comparison of experimental m/z ratios with values from the MSProduct program from Protein Prospector <http://prospector.ucsf.edu>.

(17) Henderson, S. C.; Valentine, S. J.; Counterman, A. E.; Clemmer, D. E. *Anal. Chem.* **1999**, *71*, 291. Hoaglund, C. S.; Valentine, S. J.; Sporerleder, C. R.; Reilly, J. P.; Clemmer, D. E. *Anal. Chem.* **1998**, *70*, 2236.

(18) Counterman, A. E.; Valentine, S. J.; Srebalus, C. A.; Henderson, S. C.; Hoaglund, C. S.; Clemmer, D. E. *J. Am. Soc. Mass Spectrom.* **1998**, *9*, 743.

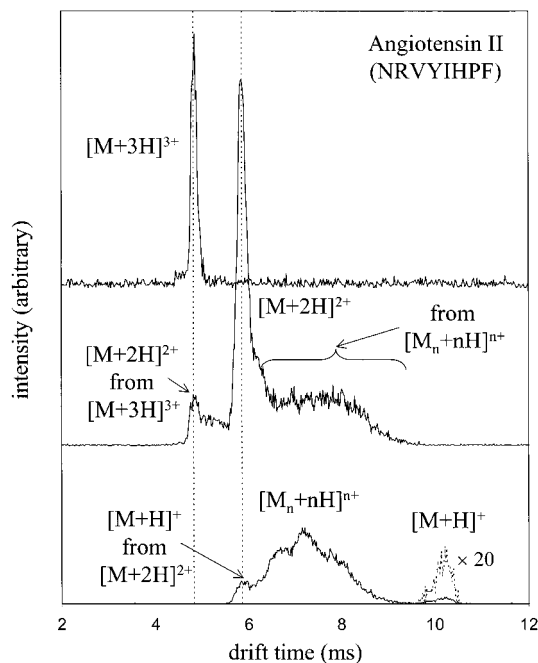


Figure 4. Drift time distributions for the $[M + 3H]^{3+}$ ($m/z = 349.5$, top), $[M + 2H]^{2+}$ ($m/z = 523.8$, middle), and $[M_n + nH]^{n+}$ ($m/z = 1046.5$, bottom) ions of angiotensin II. The vertical dashed lines at 4.82 and 5.86 ms correspond to the drift times of the $[M + 3H]^{3+}$ and $[M + 2H]^{2+}$ ions, respectively. Proton-transfer reactions of the $[M + 3H]^{3+}$ and $[M + 2H]^{2+}$ ions give rise to the feature at 4.82 ms in the $[M + 2H]^{2+}$ spectrum (middle) and the feature at 5.86 ms in the $[M_n + nH]^{n+}$ spectrum (bottom), respectively. Evidence for conversion of multiply charged multimer ions to the $[M + 2H]^{2+}$ ion at the back of the drift tube is also shown in the middle spectrum. Data were recorded using an injection voltage of 130 V, a drift field of $12.9 \text{ V}\cdot\text{cm}^{-1}$, a buffer gas pressure of 1.12 Torr (argon) and an OSC potential of 5 V. The feature in the lower drift time distribution trace shown as a dashed line corresponds to arrival of $[M + H]^+$ ions.

reported previously in a number of similar systems—that multiply charged multimers can be hidden in low-resolution mass spectra.¹⁸ From our previous work on similar systems, we assign the distribution of higher mobility ions (having $\sim 6\text{--}9\text{-ms}$ drift times, Figure 4) to a series of related unresolved multiply charged multimers having the general formula $[M_n + nH]^{n+}$. The average value of the single proton per monomer unit is consistent with the experimental $m/z = 1046.5$ value.

The process used to assign the small (unresolved) feature at 5.86 ms (as well as features in the $m/z = 523.8$ data) was more subtle. We began assigning this feature by noting that while most of the general characteristics of these data were the same as those found in data we had recorded previously without the OSC region, some new features were apparent. Upon examining the system in detail, we do not believe that the $m/z = 1046.5$ feature at 5.86 ms is due to a multiply charged multimer. Instead, it appears it arises from proton transfer of the $[M + 2H]^{2+}$ ion at the exit of the drift tube. That is, these ions have traveled through the drift tube as $[M + 2H]^{2+}$ ions and then are converted to $[M + H]^+$ as they exit the drift tube. Similar behavior is observed for features in the $m/z = 523.8$ distribution. Here, the large peak has a drift time (5.86 ms) that is consistent with the anticipated drift time for $[M + 2H]^{2+}$; the feature at 4.82 ms in the $m/z = 523.8$ distribution is coincident with the sharp peak at 4.82 ms in the $m/z = 349.5$ data set that is assigned to $[M + 3H]^{3+}$. Thus, the

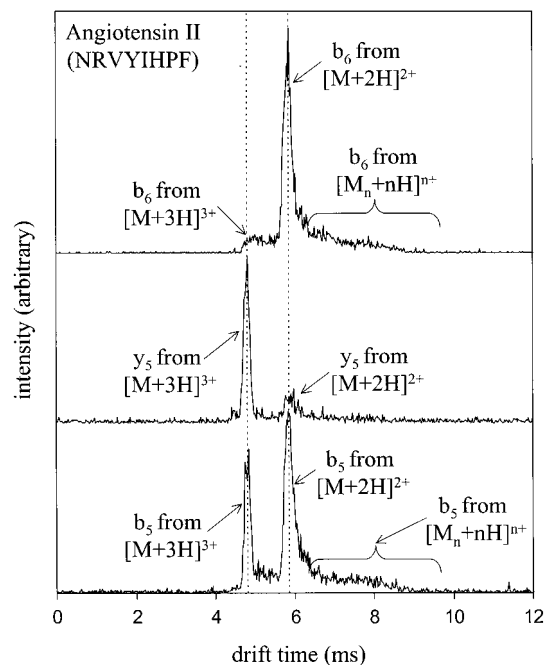


Figure 5. Parent ion mobility distributions associated with formation of the b_6 ($m/z = 784.4$, top), y_5 ($m/z = 676.4$, middle), and b_5 ($m/z = 647.4$, bottom) selected fragments of angiotensin II. See text for experimental details. The dashed lines indicate the drift times recorded in Figure 4 for the $[M + 3H]^{3+}$ and $[M + 2H]^{2+}$ parent ions (at 4.82 and 5.86 ms, respectively). The top spectrum shows that most of the b_6 fragment ions come from the $[M + 2H]^{2+}$ parent ions. The center spectrum shows that most of the y_5 fragment ions originate from the $[M + 3H]^{3+}$ parent ions. The bottom spectrum shows that b_5 fragments originate from dissociation of roughly equal abundances of the $[M + 2H]^{2+}$ and $[M + 3H]^{3+}$ parents. The experimental conditions in the drift tube are the same as in Figure 4. An OSC potential of 30 V was used to induce dissociation.

smaller $m/z = 523.8$ peak at 4.82 ms appears to arise from proton transfer of the $[M + 3H]^{3+}$ ion at the exit of the drift tube. Finally, we note that the broad feature observed in the $m/z = 523.8$ distribution appears to come about from dissociation of multiply charged multimers.

Precursor Ion Mobility Spectra for Angiotensin II Fragment Ions Formed at High OSC Potentials. Examination of the ion mobility distributions for the parent ions associated with specific fragment ions (formed at high OSC potentials, and selected with the quadrupole) provides insight into the origin of specific fragment ions that are formed in the OSC region. Figure 5 shows several typical PIM data sets for fragments that were observed in the mass spectrum of Figure 3. In this system, the PIM distribution for the b_6 fragment ion ($m/z = 784.4$) is dominated by a peak at 5.86 ms, a value that is coincident with the measured drift time for the $[M + 2H]^{2+}$ ion. This coincidence (and the similarities in the shapes of drift time peaks for these ions) indicates that b_6 ions are formed primarily from the doubly charged $[M + 2H]^{2+}$ monomer ion. A much smaller peak is observed at 4.82 ms; this can be assigned to b_6 formation from dissociation of the $[M + 3H]^{3+}$. Additionally, a small nonzero tail extends from the main peak to ~ 9 ms. This tail suggests that multiply charged multimers can also dissociate to form the b_6 fragment—although, this process is relatively inefficient.

In contrast, the dominant peak associated with the PIM data set for the y_5 fragment ion ($m/z = 676.4$) is observed at a drift

Table 1. Relative Efficiencies of Fragment Ion Formation (Angiotensin II)

selected fragments		relative efficiencies of precursor ion fragmentation ($[M + 3H]^{3+}/[M + 2H]^{2+}$) in forming specific fragments ^c
m/z^a	fragment ^b	
784	b ₆	0.8
756	a ₆	0.7
676	y ₅	14
647	b ₅	2.4
619	a ₅	1.5
534	b ₄	4.0
506	a ₄	1.0
400	y ₃	3.1
371	b ₃	2.2
343	a ₃	3.6
272	b ₂	6.7
263	y ₂	1.3

^a m/z ratios correspond to values used to select fragments for PIM studies. ^b Assigned fragment (see text for details). ^c Relative efficiency of forming specific fragments from the $[M + 2H]^{2+}$ and $[M + 3H]^{3+}$ ions. Values are determined by combining abundance information from PIM distributions and mass spectra recorded under low OSC potential conditions.

time of 4.82 ms—coincident with the $[M + 3H]^{3+}$ precursor. The fraction of $[M + 2H]^{2+}$ ions (observed from the peak at 5.86 ms) giving rise to the y₅ fragment is substantially smaller. Finally, Figure 5 also shows the PIM distribution for the b₅ fragment ion ($m/z = 647.4$). This distribution shows peaks at 4.82 and 5.86 ms. Here, the relative abundance of the b₅ fragment ions originating from the $[M + 3H]^{3+}$ and $[M + 2H]^{2+}$ ions appears to be similar with minimal fragment contribution from the multimeric species.

An understanding of the relative efficiency of the different precursor ions in forming specific fragment ions can be obtained by scaling the relative abundances associated with different peaks in the PIM data by the mass spectral peak intensities associated with the precursor ions. For example, the PIM distribution for the y₅ ion in Figure 5 shows that the peak associated with dissociation of the $[M + 3H]^{3+}$ ion has an integrated intensity that is a factor of ~ 3 times higher than contributions from dissociation of the $[M + 2H]^{2+}$ precursor. When this is combined with the observation that the abundance of $[M + 3H]^{3+}$ precursor ions is ~ 5 times less than $[M + 2H]^{2+}$ (Figure 3), we see that, under the present experimental conditions, the efficiency of forming the y₅ fragment from $[M + 3H]^{3+}$ is ~ 14 times greater than from $[M + 2H]^{2+}$. Other fragmentations are clearly favored from different precursors.

Table 1 provides a summary of information regarding the relative efficiency of producing specific angiotensin II fragments from $[M + 2H]^{2+}$ and $[M + 3H]^{3+}$ charge states. In most cases, it appears that $[M + 3H]^{3+}$ ions dissociate more efficiently than $[M + 2H]^{2+}$. We note that the collision energies associated with the OSC region are proportional to each ion's charge state. Thus, the relative enhancement of fragment formation from $[M + 3H]^{3+}$ may (at least in part) be explained by differences in the energy that is accessible for fragmentation.

Mass Spectra, Ion Mobility Distributions, and PIM Data for Electrosprayed [Sar¹, Val⁵, Ala⁸] Angiotensin II. Figure 6 shows mass spectra for the [Sar¹, Val⁵, Ala⁸] angiotensin II system at 5- and 30-V OSC potentials. Overall, these data appear similar to those shown for angiotensin II. At low OSC potentials, the

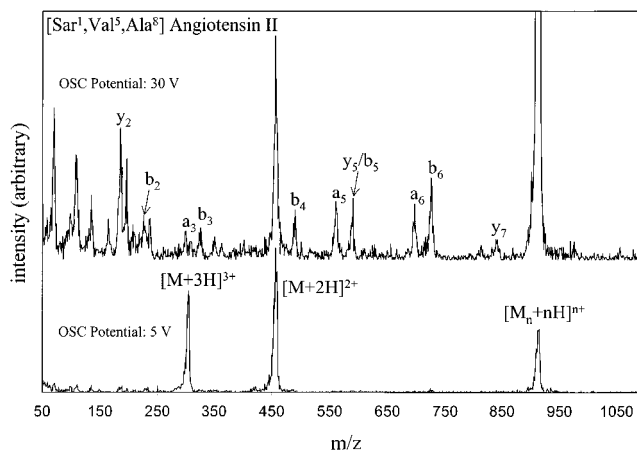


Figure 6. Mass spectra for [Sar¹, Val⁵, Ala⁸] angiotensin II at two different OSC potentials. The bottom spectrum was recorded using an OSC potential of 5 V and is dominated by peaks corresponding to the $[M_n + nH]^{n+}$, $[M + 2H]^{2+}$, and $[M + 3H]^{3+}$ ions. The top spectrum (showing many fragment peaks) was recorded using an OSC potential of 30 V.

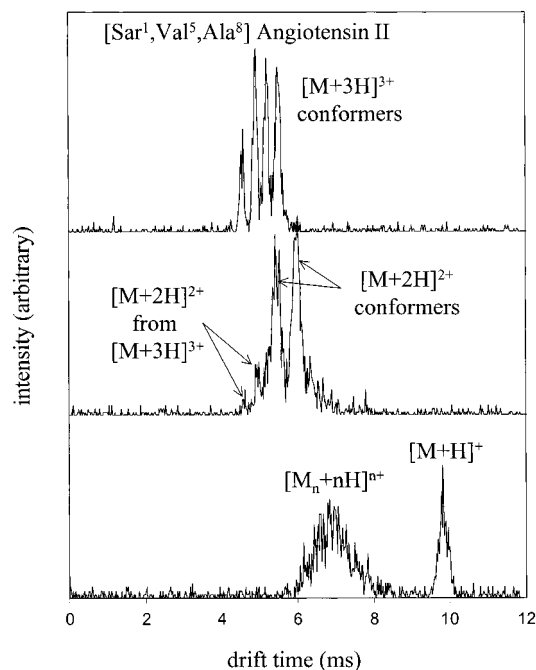


Figure 7. Drift time distributions for selected $[M + 3H]^{3+}$ ($m/z = 305.2$, top), $[M + 2H]^{2+}$ ($m/z = 457.3$, middle), and $[M_n + nH]^{n+}$ ($m/z = 913.5$, bottom) ions of [Sar¹, Val⁵, Ala⁸] angiotensin II. Four distinct conformers are apparent for the $[M + 3H]^{3+}$ ion. The $[M + 2H]^{2+}$ ion gives rise to two distinct conformers with additional peaks arising from proton transfer of multiple $[M + 3H]^{3+}$ conformers. Data were recorded using an injection voltage of 130 V, a drift field of 12.9 V·cm⁻¹, an argon buffer gas pressure of 1.12 Torr, and an OSC potential of 5 V.

distribution is dominated by peaks centered at $m/z = 913.5$, 457.3, and 305.2, corresponding to the $[M + H]^+$ (and multiply charged multimers), $[M + 2H]^{2+}$, and $[M + 3H]^{3+}$ ions, respectively. At an OSC potential of 30 V, a series of a-, b-, and y-type fragments is observed.

Figure 7 shows ion mobility distributions of the nominal $[M + H]^+$ (i.e., $m/z = 913.5$), $[M + 2H]^{2+}$, and $[M + 3H]^{3+}$ ions obtained using OSC conditions of 5 V. The distribution for the $m/z = 913.5$ ions shows a peak that corresponds to the singly

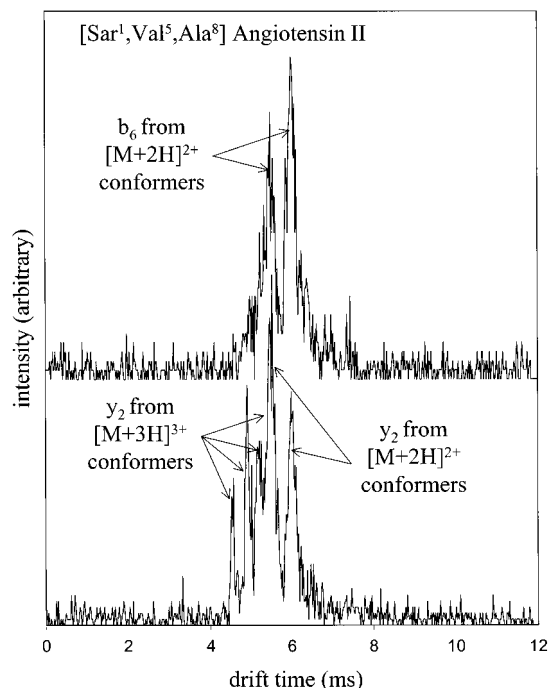


Figure 8. Parent ion mobility distributions for selected b_6 ($m/z = 784.4$, top) and y_2 ($m/z = 263.1$, bottom) fragments of [Sar¹, Val⁵, Ala⁸] angiotensin II. The top spectrum shows that the b_6 fragment ion is formed from both conformations of $[M + 2H]^{2+}$. The bottom spectrum shows that the y_2 fragment ion is formed from multiple conformers of both the $[M + 2H]^{2+}$ and $[M + 3H]^{3+}$ ions. The experimental conditions associated with the mobility separation were identical to those in Figure 7. The OSC potential was 30 V.

charged monomer as well as a broad feature associated with higher mobility $[M_n + nH]^{n+}$ ions—behavior that is similar to the description given above for the angiotensin II system. Ion mobility distributions for the $[M + 2H]^{2+}$ and $[M + 3H]^{3+}$ are somewhat remarkable; each of these ions exhibits resolvable geometric structures that do not interconvert during the millisecond time scales of these experiments. Because they have different shapes, we refer to the multiple structures as different conformations (although the different shapes may arise from different protonation site configurations). Under the present conditions, at least two conformations are observed for $[M + 2H]^{2+}$ ions, and $[M + 3H]^{3+}$ ions can form at least four distinct structures.

At higher OSC potentials it is possible to investigate the fragmentation of different conformations of the [Sar¹, Val⁵, Ala⁸] angiotensin II charge states. The idea that different ion conformation types of peptides and proteins might lead to specific fragmentation patterns is currently receiving considerable attention.¹⁹ The present approach provides a means of directly assessing the fragmentation patterns associated with multiple ion conformations that have identical sequences. Figure 8 shows PIM data obtained for the b_6 and y_2 fragment ions that are observed

in the mass spectrum shown in Figure 6. The PIM data for the b_6 fragment ion shows two peaks at 5.48 and 6.00 ms—these drift times and the shapes of the peaks are indistinguishable from those observed for the $[M + 2H]^{2+}$ parent. It is especially interesting that the relative contributions to formation of the b_6 ion from both $[M + 2H]^{2+}$ conformations appear to be equal. The PIM distribution recorded for formation of the y_2 ion shows that doubly and triply charged peptide ions dissociate to form this fragment. This data set shows that five peaks associated with populations of the two different $[M + 2H]^{2+}$ conformers and four distinct $[M + 3H]^{3+}$ conformers are observed. Note, that the highest mobility $[M + 2H]^{2+}$ and lowest mobility $[M + 3H]^{3+}$ conformers are observed at nearly identical drift times (5.48 and 5.50 ms, respectively) and thus appear to overlap in the PIM data for the y_2 ion. Examination of the relative intensities of the different peaks in Figure 8 indicates that all conformers dissociate to form the y_2 ion; additionally, under the conditions employed, we find no evidence for preferential dissociation of any specific conformers.

A caveat associated with the inability to observe any differences in conformer dissociation is that structures may interconvert rapidly (especially when exposed to energizing collisions) prior to dissociation. Thus, we cannot distinguish between a mechanism in which each conformer dissociates directly to products or one where all conformers are transformed into a similar predissociative state prior to decomposition. Further studies in our laboratory are directed at investigating the dissociation of specific conformations for this and several larger peptide and protein systems in more detail.²⁰ On the basis of results from other laboratories,¹⁹ it seems likely that some types of conformations (resolvable by mobility separations) will exhibit unique dissociation behavior.

SUMMARY AND CONCLUSIONS

A new ion mobility-mass spectrometry approach that incorporates a high-pressure focusing element and a differentially pumped OSC region at the exit of the drift tube is described. The approach has several advantages. Ion transmission is improved by factors of ~ 5 – 10 compared with previous flat plate designs—a result that is rationalized by noting the focusing properties of a conical drift tube exit lens as well as the increased hole size that is made possible because of the differential pumping region. Additionally, by varying the potential across the differential pumping region, it is possible to examine the fragmentation pathways of mobility-selected ions. The latter approach is analogous to OSC dissociation that is often used in electrospray sources. The ability to examine the mobilities of parent ions associated with specific fragments provides detailed insight into the origin of OSC fragments. Here, we presented examples that have explored how different ion charge states as well as different conformations contributed to production of specific fragments.

The present experimental approach utilized an OSC region at the exit of an injected-ion mobility drift tube. In this instrumental design, the ESI source is separated from the drift tube and ions are extracted into a vacuum and then injected into the drift tube prior to mobility separation and subsequent OSC fragmentation analysis. Recently several groups have developed high-pressure

(19) Vachet, R. W.; Asam, M. R.; Glish, G. L. *J. Am. Chem. Soc.* **1996**, *118*, 6252. Schnier, P. D.; Price, W. D.; Jockusch, R. A.; Williams, E. R. *J. Am. Chem. Soc.* **1996**, *118*, 7178. Zubarev, R. A.; Kruger, N. A.; Fridriksson, E. K.; Lewis, M. A.; Horn, D. M.; Carpenter, B. K.; McLafferty, F. W. *J. Am. Chem. Soc.* **1999**, *121*, 2857. Tsapralis, G.; Nair, H.; Somogyi, A.; Wysocki, V. H.; Zhong, W.; Futrell, J. H.; Summerfield, S. G.; Gaskell, S. J. *J. Am. Chem. Soc.* **1999**, *121*, 5142 and references therein. Schaaff, T. G.; Cargile, B. J.; Stephenson, J. L., Jr.; McLuckey, S. A. *Anal. Chem.* **2000**, *72*, 899. Horn, D. M.; Ge, Y.; McLafferty, F. W. *Anal. Chem.* **2000**, *72*, 4778.

(20) Hoaglund-Hyzer, C. S.; Lee, Y. J.; Clemmer, D. E., work in progress.

drift tubes in which ions are electrosprayed directly into the high-pressure region of the mobility apparatus.^{18,21} Incorporation of the differentially pumped OSC region at the exit of a high-pressure drift tube should offer improvements in signal intensities as well as the ability to examine the origin of fragments generated in the OSC region. Coupling such an approach to most mass analyzers

should also be relatively simple—comparable with the use of OSC dissociation with ESI. We are currently incorporating such a source for our high-pressure drift tube.

ACKNOWLEDGMENT

The authors gratefully acknowledge support of this work through grants from the National Institutes of Health (1R01GM59145-01 and -55647-03) and the National Science Foundation (CHE-0078737).

Received for review March 13, 2001. Accepted May 15, 2001.

AC010295E

(21) Wittmer, D.; Chen, Y. H.; Luckenbill, B. K.; Hill, H. H., Jr. *Anal. Chem.* **1994**, *66*, 2348. Chen, Y. H.; Hill, H. H., Jr.; Wittmer, D. P. *Int. J. Mass Spectrom. Ion Processes* **1996**, *154*, 1. Hudgins, R. R.; Woenckhaus, J.; Jarrold, M. F. *Int. J. Mass Spectrom. Ion Processes* **1997**, *165/166*, 497. Guevremont, R.; Siu, K. W. M.; Wang, J.; Ding, L. *Anal. Chem.* **1997**, *69*, 3959. Wu, C.; Siems, W. F.; Asbury, G. R.; Hill, H. H., Jr. *Anal. Chem.* **1998**, *70*, 4929.